

Importance of the Nature of the Active Acid/Base Pairs of Hydroxyapatite Involved in the Catalytic Transformation of Ethanol to *n*-Butanol Revealed by *Operando* DRIFTS

Manel Ben Osman,^[a] Jean-Marc Krafft,^[a] Cyril Thomas,^[a] Tetsuya Yoshioka,^[b] Jun Kubo,^[b] and Guylène Costentin^{*,[a]}

Operando DRIFTS is used to identify the nature and the role of the surface sites of hydroxyapatites (HAPs) involved in the catalytic transformation of ethanol to *n*-butanol. The surface processes occurring upon a first reaction step followed by a step under He flow greatly influence the reactivity of HAPs in a subsequent second reaction step. Ethanol is found to be mostly activated by the basic OH[−] groups of HAPs, as indicated by the concomitant recovery of ethanol conversion and OH[−] groups under He flow. The drastic changes in selectivity observed during the second reaction step reveal the key role of acidic

sites cooperatively acting with basic sites for basic reaction steps. Once the POH groups are poisoned by extensive formation of polymeric carbon species and the Ca²⁺ sites are available, the production of acetaldehyde is drastically promoted at the expense of that of *n*-butanol. It is concluded that i) acetaldehyde acts as an intermediate in the formation of *n*-butanol, and ii) various active sites are involved in the key basic reaction steps such as Ca²⁺–OH[−] and POH–OH[−] acid-base pairs in the dehydrogenation of ethanol to acetaldehyde and the aldol condensation for *n*-butanol formation, respectively.

Introduction

In the context of growing production of ethanol from biomass, its valorization into higher value chemicals such as ethylene, 1,3-butadiene and *n*-butanol has attracted much attention recently.^[1] Besides being an important industrial chemical for paints and polymers, as well as a solvent,^[2] *n*-butanol is also considered as a potential gasoline fuel additive^[1a,3] due to its higher energy density and its lower miscibility in water relative to ethanol.^[4] Butanol is commonly produced *via* the hydroformylation reaction (oxo process) followed by a hydrogenation step. Yet these processes require fuel-derived feedstocks and severe operating conditions leading to high operating costs.^[5] Recently, it was shown that *n*-butanol can be alternatively produced *via* the coupling of ethanol molecules over a wide variety of catalysts,^[3a,6] among which the hydroxyapatite (HAPs) system appeared to be very attractive due to its high activity and selectivity.^[4,6a,7]


Although still debated in the literature, it is commonly reported that the ethanol coupling to *n*-butanol occurs via a Guerbet-type mechanism.^[7a,b,d] In the related Guerbet transformation,^[8] an ethanol molecule is firstly dehydrogenated into acetaldehyde. Acetaldehyde then reacts via an aldol condensa-

tion reaction to form unsaturated condensation products that are eventually hydrogenated to *n*-butanol,^[9] possibly via a Meerwein-Ponndorf-Verley-like mechanism.^[10] This pathway is supported by recent kinetic studies,^[4] in which adsorbed acetaldehyde species have been revealed as intermediates. Combining thermodynamic and kinetic data, Scalbert et al. concluded that *n*-butanol is both a primary product resulting from a “direct” bimolecular route (minor fraction) and a secondary product.^[7c] Such a “direct” bimolecular route was also claimed for the K–Cu/MgCeO_x system.^[11] According to Scalbert et al., the main “indirect” route to *n*-butanol would result from the condensation of acetaldehyde and ethanol, rather than from the self-condensation of acetaldehyde.^[7c] Further insights into the understanding of the mechanism of formation of *n*-butanol from ethanol would require the identification of the nature of the active sites involved in the transformation of ethanol to *n*-butanol of the hydroxyapatite system. To date, it is assumed that the Guerbet coupling reaction requires weak acid-base bifunctional catalysts with a “proper balance of acid-base site pairs”, that might explain the better catalytic performance of HAPs compared to MgO.^[4a] Finally, it was reported recently that the active sites involved in the formation of acetaldehyde and *n*-butanol are different.^[4b]

Hydroxyapatite (Ca₁₀(PO₄)₆(OH)₂ generic formula) is a well-known calcium phosphate compound that is also the main mineral component of bones and teeth. This biocompatible, ecofriendly and harmless material was recently found of interest in heterogeneous bifunctional^[12] and acid-base catalysis,^[7a,13] thanks to its synthesis-dependent tunable properties.^[14] It was found that changes in the Ca/P bulk ratio influence the surface reactivity to a significant extent.^[14a,15] Ca/P ratios lower than the stoichiometric ratio, i.e. 1.67, would favor acidity, while higher Ca/P ratios would rather promote basicity.^[7a,16] Note, however,

[a] M. B. Osman, J.-M. Krafft, C. Thomas, G. Costentin
Laboratoire Réactivité de Surface, LRS
Sorbonne Université, CNRS
75005 Paris (France)
E-mail: guylene.costentin@upmc.fr

[b] T. Yoshioka, J. Kubo
Central Research Center
Sangi Co., Ltd.
Fudooino 2745-1, Kasukabe-shi, Saitama 344-0001 (Japan)

 Supporting information for this article is available on the WWW under <https://doi.org/10.1002/cctc.201801880>

that the acid-base properties of HAPs do not always follow the above-mentioned guidelines based on the Ca/P ratio, especially when comparing hydroxyapatite samples prepared under different conditions.^[14b] It must be stressed that the Ca/P ratio does not only depend on the calcium content of the sample but also on its phosphorus content as phosphates, which itself strongly depends on the presence of carbonates. In addition, the Ca/P bulk ratio does not account for the OH concentration. The latter was shown to be influenced to a significant extent by the presence of structural defects, as illustrated by the more general formula of HAPs: $\text{Ca}_{10-x-B}(\text{PO}_4)_{6-x-B}(\text{HPO}_4)_x(\text{CO}_3)_{A+B}(\text{OH})_{2-x-2A-B}$ in which A and B are related to carbonates located on hydroxyl and phosphate structural sites, respectively.^[17] The concentration of OH groups was thus found to be a more relevant descriptor than the Ca/P ratio to account for the basic reactivity of HAPs.^[14b] The discrimination between bulk and surface species remains complex and investigations aiming at characterizing the surface at a molecular level are needed to identify the nature of the surface sites likely involved in acid-base catalysis. Bulk hydroxyl (OH) and hydrogenophosphate (POH) species could be discriminated recently from their surface species by FTIR and NMR using isotopic labelling.^[18] The infrared fingerprints and relative thermal stabilities of A- and B-type bulk and surface carbonates have also been reported.^[17] From the latter IR study, it was found that surface carbonates and hydrogenocarbonates are formed upon CO_2 adsorption, which reveals the presence of potential Lewis basic sites such as PO_4 and OH groups emerging from the channels running along the *c*-axis.^[17] However, when Brønsted basicity is involved, (ability to interact with a proton donor molecule such as acetylene),^[17] an acid-base pair is required.^[19] In such a case, only the OH groups were found to be involved in the adsorption processes. This can be explained by the fact that surface phosphate groups from phosphate-rich terminations^[20] are protonated to POH groups to ensure the surface charge balance.^[21] Such a conclusion is supported by an earlier study in which Brønsted acidity was revealed by means of the adsorption of CO, which is a basic probe molecule.^[7e] These surface-terminating POH groups were found to be much more accessible than Ca^{2+} Lewis acid sites, whose limited surface concentration was further confirmed by complementary XPS and ISS measurements.^[7e] Consequently, the POH groups are likely involved as the acidic partners of the acid-base pairs interacting with a proton donor molecule, such as acetylene.^[17] Moreover, increasing the relative POH to calcium content of the top surface by modulation of the synthesis parameters was found to be beneficial to the basic reactivity of HAPs^[7e] as measured by a model reaction such as the conversion of the 2-methyl-3-butyn-2-ol (MBOH).^[22] Such an increase in the relative POH to calcium content of the top surface of HAPs was also found to promote ethanol conversion and this was assigned to an appropriate acid-base balance.^[7e] Ho et al. suggested that Ca–O and $\text{CaO}/\text{PO}_4^{3-}$ pairs would be involved in the transformation of ethanol to *n*-butanol as active sites for the dehydrogenation and aldol condensation steps, respectively.^[4b] Such a proposal remains uncertain when considering the structural properties of HAPs, for which no evident Ca–O-like species are present due to the facts that

oxygen atoms in these materials belong to phosphate and hydroxyl groups, and the surface concentration in Ca^{2+} is limited.^[7e] In contrast, the potential involvement of surface terminated acidic POH and basic OH groups has not been considered yet to our knowledge, even if it was recently reported that HAPs are much more active and selective in *n*-butanol compared to other calcium phosphates.^[23]

The *operando* DRIFT studies reported in the present article aim at investigating the nature and the role of the acidic and basic surface sites involved in the transformation of ethanol to *n*-butanol. For this purpose, hydroxyapatite samples with various Ca/P ratios are investigated and the influence of the activation temperature is also addressed for one particular sample. The modifications occurring on the related hydroxyapatite surfaces after their thermal activation are followed *operando* (reaction 1). In order to ascribe the perturbations of the surface vibrators to the catalytic active sites involved in the conversion of ethanol into acetaldehyde and *n*-butanol and/or to sites involved in deactivation processes, a further treatment under He flow was carried out at the reaction temperature before a second reaction step (reaction 2) was performed.

Results and Discussion

1. Initial Surface States

Absolute DRIFT spectra recorded at the end of the activation step are shown in Figure 1. A corresponding representation of the related hydroxyapatite surface is reported in Figure 2 A.

1.1 Carbonation

Figure 1 A shows that the HAP samples exhibit bulk A-type carbonates (1414 , 1444 and 1505 cm^{-1}) and few amounts of B-type carbonates, (1456 and 1545 cm^{-1}).^[17] Due to their low thermal stability, surface carbonates formed on phosphate groups and expected at 1485 and 1385 cm^{-1} ^[17] vanish upon thermal pretreatment at 623 and 873 K . An additional band is also observed at 1577 cm^{-1} , which relative intensity decreases as the Ca/P ratio decreases. This band, which is ascribed to the ν_{OCO} vibrator of surface unidentate calcium carbonates,^[24] vanishes upon activation at 873 K .

1.2 Hydroxylation

1.2.1 Hydroxyls from the Channels

All of the HAP samples exhibit an intense absorption band at 3566 cm^{-1} (Figure 1 B). This band is attributed to the ν_{OH} vibrator of both bulk hydroxyl groups located in the channels running along the *c*-axis and to their top surface fraction.^[18a] Compared to spectra recorded at RT,^[18a] the spectra recorded at 623 K reveal an additional ν_{OH} contribution at 3534 cm^{-1} . The intensity of the band at 3566 cm^{-1} decreases whereas the

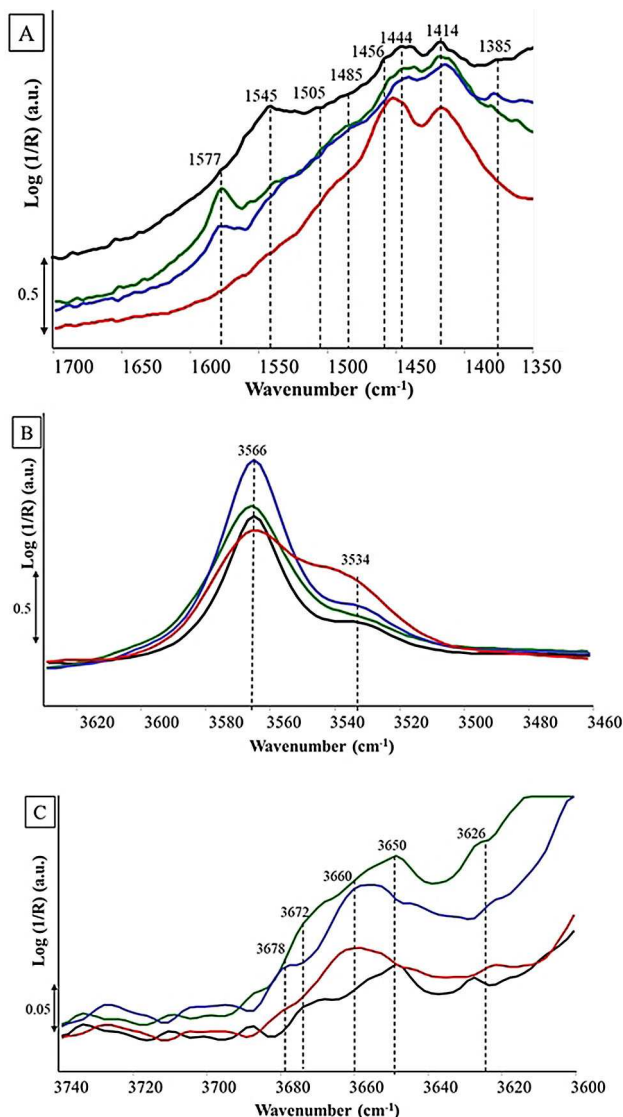


Figure 1. Absolute DRIFT spectra of HAP-S_{623 K} (blue), HAP-U_{623 K} (black), HAP-O_{623 K} (green) and HAP-O_{873 K} (red) recorded at 623 K at the end of the activation step in the A) $\nu_{\text{CO}_3^-}$ B) ν_{OH} and C) $\nu_{\text{PO-H}}$ regions.

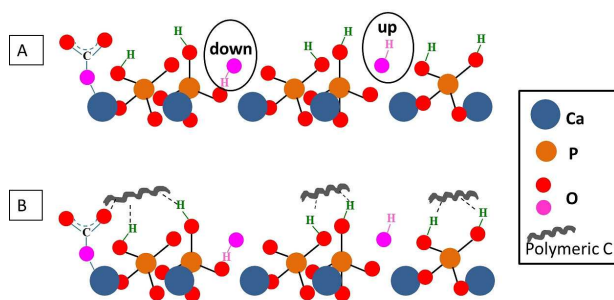


Figure 2. Schematic representation of the terminated surface of HAPs (A) freshly activated surface with up and down orientation for the protons of the basic OH groups, protonation of phosphate groups and unidentate calcium carbonates and (B) modified surface upon poisoning of the POH and unidentate calcium carbonates groups by carbon polymeric species.

intensity of the shoulder at 3534 cm^{-1} increases upon thermal activation at 623 K (not shown). As shown in Figure 1 B (green and red spectra), such a tendency is found to be promoted by activation at 873 K. The band at 3534 cm^{-1} results from a dehydroxylation process in the channels, associated to thermally activated proton migration.^[25] This process leads to the formation of few O^{2-} ions inside the columns. Hence, as supported by analogy with earlier studies performed on fluorinated HAPs,^[26] the band at 3534 cm^{-1} is assigned to ν_{OH} vibrators H-bonded to the generated O^{2-} species. It indirectly indicates the presence of O^{2-} species in the hydroxyapatite channels, mostly as bulk species, but also possibly as surface species emerging from the channels, as shown below.

1.2.2 Terminated POH Groups

Besides the bands associated to the OH groups from the channels, other low intensity ν_{OH} bands are detected at higher wavenumbers (Figure 1 C). The bands at 3678, 3672, 3660 and 3626 cm^{-1} are associated to terminating protonated phosphate groups located on the surface, whereas that at 3650 cm^{-1} originates from defective hydrogenophosphate groups present in the bulk.^[14b,18a] The slight modifications of the shape of the spectra in this region are significant of different relative intensities for the various contributions. The origin of such a multiplicity of surface POH contributions is probably due to the presence of phosphate rich terminations with slightly different relaxation processes, and possibly to different protonation level of these phosphates.

2. Reaction 1 Step

2.1 Gas Phase Analysis

It was shown earlier that catalytic performance measured in the DRIFT cell reactor was representative of that measured in a conventional reactor for similar contact times,^[7e] even though lower conversions may be achieved compared to the conventional reactor probably due to differences in reactor geometry. Ethanol conversion decreases drastically for all of the samples within the 5 first minutes on stream (Figure 3 A) and then much more slowly. Among the samples activated at 623 K, the stoichiometric HAP-S_{623 K} and over-stoichiometric HAP-O_{623 K} samples exhibit similar initial ethanol conversion (after 2 min on stream), whereas the under-stoichiometric HAP-U_{623 K} sample appears to be less active. This ranking is maintained after 50 min on stream. Overall, after activation at 623 K, HAP-S_{623 K} seems to be the most active sample in agreement with earlier studies.^[7a] This ranking (same than that obtained with U-type conventional reactor) is fully consistent with the ranking obtained for the basic reactivity evaluated by means of the MBOH model reaction^[22] (SI 1 Figure S1a). The present study therefore provides an additional support for a correlation already evidenced between the MBOH and ethanol conversions, as reported earlier.^[7e] In these earlier studies, it was proposed

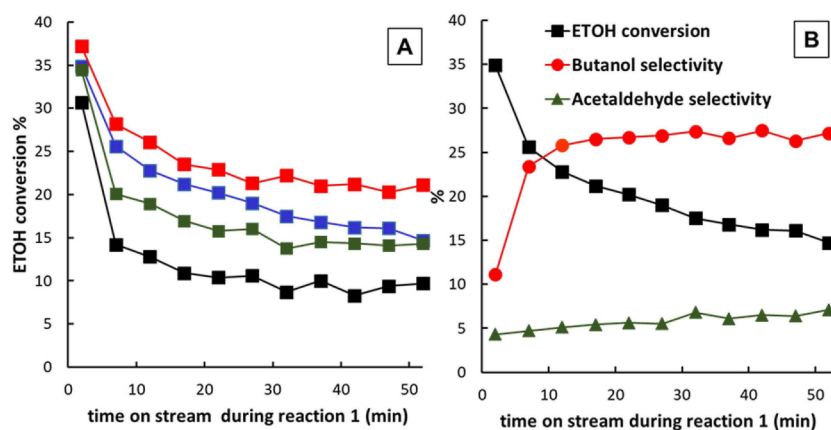


Figure 3. Reaction 1 step: (A) Evolution of the ethanol conversion upon time on stream for HAP-S_{623 K} (blue), HAP-U_{623 K} (black), HAP-O_{623 K} (green) and HAP-O_{873 K} (red), (B) evolution of the ethanol conversion and the selectivity in the main detected products upon time on stream for the HAP-S_{623 K} sample.

that similar acid-base pairs were involved in the rate determining step of the two reactions,^[7e] which is likely to be the aldol condensation in the case of the ethanol condensation reaction.^[4b,7b] As already reported for HAPs samples^[4,6a,7c-e] and for the present samples tested in a U-type conventional reactor,^[7e] Figure 3 B shows that, beside acetaldehyde, which selectivity remains quite low (~7%), and very few amount of ethylene, the main reaction product is found to be *n*-butanol. Its production results from a quite complex reaction network including sequential steps that also lead to the formation of various products: other C₄- compounds such as 3-butene-2-ol, 3-butene-1-ol, 2-methyl-2-propene-1-ol, 1,3-butadiene and diethyl ether and C₆- compounds (2-ethylbutanol and hexanol).

As illustrated for HAP-S_{623 K}, *n*-butanol selectivity rapidly increases within the 5 first minutes on stream (Figure 3 B) and then stabilizes around 25%. The lower *n*-butanol selectivity compared to the earlier studies performed in a conventional reactor^[7e] (~50–60% depending on the HAPs stoichiometry) may be attributed to the low flow rate that had to be used in the present study due to the limited amount of sample introduced in the DRIFT cell. Such operating conditions were shown to favor secondary reactions.^[4a] Here, they even hinder the desorption of heavy products being responsible of the decrease of *n*-butanol and other heavy products evolved in gas phase, and hence accounting for the gas-phase carbon deficit observed in the present operando experiments. Due both to these phenomena and to the different EtOH conversion levels measured for the different HAPs samples (Figure 3A), the different selectivities in C₄- compounds obtained for HAPs of various stoichiometries is rather difficult to comment.

Despite a lower surface area, HAP-O_{873 K} is the most active sample with the greatest *n*-butanol yield and the least sensitive to deactivation (Figure 3 A). Such a positive effect of the high activation temperature has not been reported to date in the transformation of ethanol to our knowledge. Similar trends were also obtained for HAP-S and when characterizing these samples by means of the MBOH model reaction (SI 1 Figure S1a). Given that MBOH conversion on HAPs was shown to

be dependent on the OH⁻ concentration^[14b] and that the increase of the activation temperature favors dehydroxylation leading to the formation of O²⁻ species (Figure 2 B), these results raise the question of the role of OH⁻ versus O²⁻ in the catalytic transformation of ethanol to *n*-butanol. Ho et al. have only considered O²⁻ species as active sites,^[4b] thus neglecting the eventual involvement of OH⁻ species. Note also that in the case of the cobalt or vanadium hydroxyapatite system, specific active species derived from OH⁻ groups were proposed to favor the activation of the C–H bonds of propane.^[27]

2.2 Surface Analysis by DRIFT

The difference DRIFT spectra exhibit positive and negative contributions ascribed to the formation of newly adsorbed species and to the perturbation and/or the disappearance of pre-existing bands, respectively, as detailed below for the HAP-S_{623 K}. The assignments of the related IR bands are summarized in Table 1.

2.2.1 Newly Adsorbed Species

Figure 4 A shows the rather rapid appearance of several contributions at 2963, 2930, 2880 and 2862 cm⁻¹ under time on stream. These contributions are assigned to the vibrations of C–H groups originating from adsorbed reactant and/or products.^[28] C–O contributions of low intensity are observed at 1390–1470 cm⁻¹ together with an intense multicomponent bands around 1500–1670 cm⁻¹ gathering two main ν_{CO} contributions at 1554 and 1536 cm⁻¹ and a less intense ν_{CC} contribution at 1596 cm⁻¹ (Figure 4 B). These bands are assigned to carboxylates^[28c] possibly in heavy polymeric compounds.^[29] The increasing formation of these adsorbates contribute to the gas-phase carbon deficit (Figure 3 B) and to the deactivation process, as shown by the correlation between the evolution of the area of the 1500–1650 cm⁻¹ contributions

Table 1. Assignment of the IR bands related to vibrators originating from hydroxyapatite sites and adsorbates.

Species	Location	Vibrator	Wavenumber [cm ⁻¹]	Reference
Carbonates	bulk type A	ν_{CO}	1414	[17]
			1444	
			1505	
	bulk type B	ν_{CO}	1456	[24]
			1545	
Hydroxyls	surface (in interaction with PO_4^{3-})	ν_{CO}	1485	[26a]
			1385	
	unidentate calcium carbonates	ν_{OCO}	1577	[18a]
	bulk and surface OH of the columns	$\nu_{\text{O-H}}$	3566	
	$\text{OH}^- - \text{O}^{2-}$	$\nu_{\text{O-H}}$	3534	[26a]
	columnar OH^- in H-bonding interaction with neighboring columnar O^{2-} (bulk and surface)			
Protonated phosphates	split into 2 surface OH contributions revealed upon interaction of $\text{C}_2\text{H}_5\text{OH}$ with the surface	$\nu_{\text{O-H}}$	3568	[17]
			3560	
	terminal surface POH	$\nu_{\text{PO-H}}$	3678	[14b, 18a]
			3672	
			3660	
Ethanol and products	bulk POH adsorbed on the surface	$\nu_{\text{PO-H}}$ $\nu_{\text{C-H}}$	3626	[18a]
			3650	
			2963	
			2930	
			2880	
Carboxylates/heavy polymeric compounds	adsorbed on the surface	ν_{SCOO} ν_{asOCO} $\nu_{\text{C-C}}$	2862	[28c]
			1390–1470	
			1536, 1554	
			1596	[29]

[a] by analogy with $\nu_{\text{O-H}}$ at 3546 cm⁻¹ in hydroxyapatites modified by fluoride assigned to an $\text{OH}^- - \text{F}^-$ contribution.

and the loss of ethanol conversion upon time on stream (Figure 5). The strong adsorption of polymeric compounds is also supported by the yellow-brownish color observed for the used catalysts. Note that there is no evidence for the formation of chemisorbed water (band expected ~1640 cm⁻¹). The absence of adsorbed acetaldehyde (bands expected at 1709–1711 cm⁻¹),^[28a,b] is indicative that acetaldehyde is rapidly desorbed or transformed.

2.2.2 Perturbation of Pre-Existing Surface Species

The band at 1577 cm⁻¹ is perturbed from the first minutes on stream of the reaction 1 step (Figure 4 B). The increase in intensity of this perturbation with time on stream is in line with the involvement of an interaction of the related unidentate calcium carbonate species with adsorbates, rather than with their sudden vanishing under reactant flow.

The surface contribution of hydroxyl groups emerging from the channels is also modified (Figure 4 C). The band at 3534 cm⁻¹, which appears after the thermal activation process (Figure 1 B), is only slightly modified under reaction conditions. This is consistent with the main assignment of this contribution to OH groups H-bonded to bulk O^{2-} species. This contribution also indicates the presence of a limited fraction of the O^{2-} species on the surface and of their involvement in the catalytic reaction, as discussed below. Whereas only one contribution at 3566 cm⁻¹ could be identified from the absolute spectra of the thermally-activated surface (including both bulk and surface species) (Figure 1 B),^[18a] the exposure of the HAp surface to

ethanol and/or its products reveals two perturbed contributions at 3560 and 3568 cm⁻¹ (Figure 4 C). Such a splitting was also observed for the interaction of acetylene with the HAp surface^[17] and following the MBOH reaction under operando conditions (SI 1 Figure S1b). Several explanations can account for such a surface OH differentiation (Figure 3 A). Firstly, the existence of two different surface terminating hydroxyl groups with up and down orientations of the protons with respect to oxygen was recently evidenced in a NMR study.^[18b] Such a speciation, which cannot be seen in the absolute IR spectrum due to the much higher concentration of bulk OH species compared to surface OH species,^[18a] might be more easily observable in the difference spectra that are only sensitive to surface modifications. Such different up and down configurations might lead to slightly different basicity or accessibility and thus to slightly different reactivity. Secondly, in the context of basic reactivity, acid-base pairs are involved and one may also consider the involvement of basic OH^- species with different acidic partners (Ca^{2+} versus POH, and/or different POH species as suggested by the various surface $\nu_{\text{PO-H}}$ contributions pointed out in Figure 1 C and reported in Table 1) with different strengths resulting in the differentiation of OH^- species (Figure 2 A). Note that as reported earlier for identical materials, the accessibility of Ca^{2+} ions as potential Lewis acid sites was shown to be quite limited compared to that of POH from CO-FTIR adsorption measurements at 77 K.^[17] In the present study, this lack of accessibility may be explained by the presence of stable surface unidentate calcium carbonates. The negative contributions at 3678, 3672 and 3660 cm⁻¹ attributed to the perturbation of the surface POH vibrators (Figure 4 C) clearly

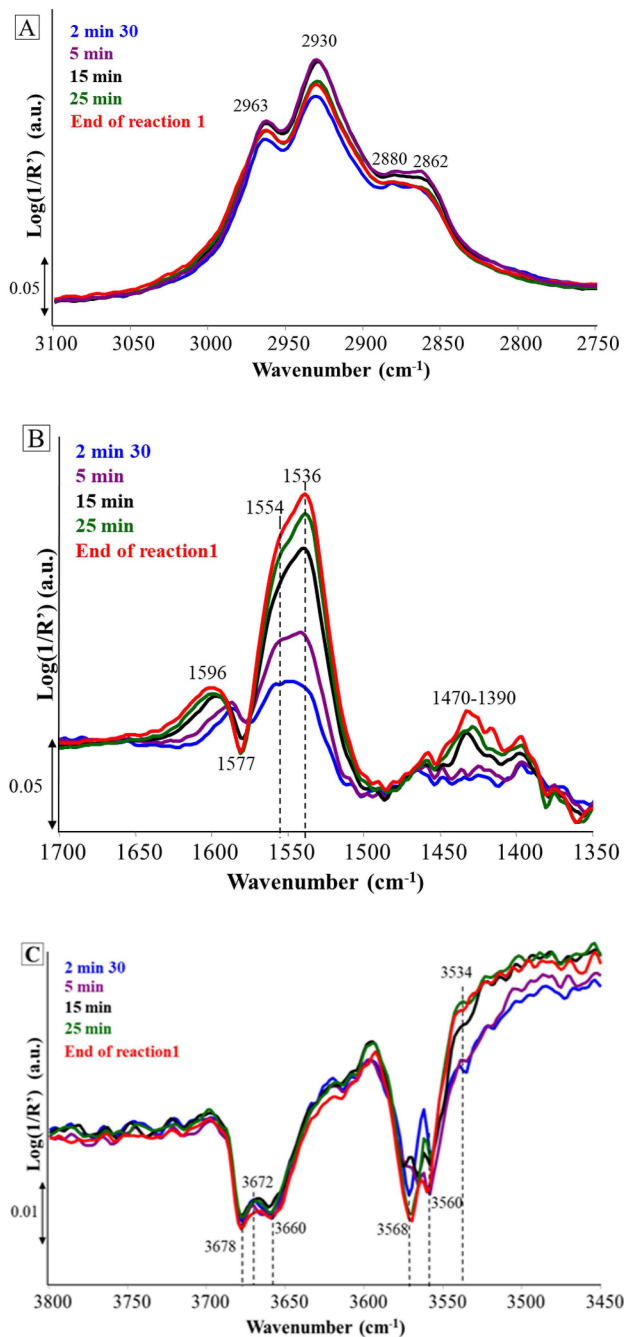


Figure 4. Difference DRIFT spectra recorded during reaction 1 for the HAp-S₆₂₃ K sample. A) ν_{CH} B) ν_{CO} and ν_{CC} and C) ν_{OH} regions.

reveal their involvement in the reaction. Note that the intensity of these perturbations (quite similar for the three components) does not match that observed on the absolute spectra shown in Figure 1 C (the intensity of the bands increases in the order $3678 < 3672 < 3660$ cm⁻¹). Similar features were obtained using acetylene and CO probes and were ascribed to different POH acidic strengths, accessibility and/or proximity with the neighboring OH surface basic sites.^[17] Interestingly, similar features are also observed following the MBOH reaction under operando conditions (SI 1 Figure S1b).

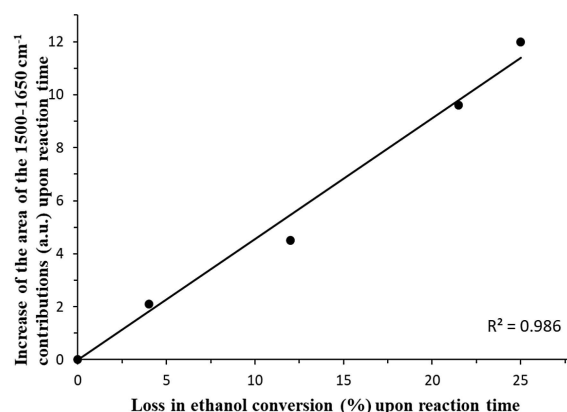


Figure 5. Correlation between the loss in ethanol conversion and the increase of the area of the contribution in the 1500–1650 cm⁻¹ range for the HAp-S₆₂₃ K sample.

2.3 Comparison of the Various HAp Samples

Overall, similar tendencies are observed for all of the HAp samples. This can be seen upon reaction time on stream in the case of the most active sample (HAp-O₈₇₃ K) (SI 2 Figure S2). Consequently, only the spectra recorded at the end of the reaction 1 step are reported here for all of the samples. The changes in intensity of the positive C–H contributions (Figure 6 A) on the difference spectra can account for the differences in conversion and deactivation profiles observed for the various samples (Figure 3 A). The intensity of the negative contributions at 1577, 3678, 3672 cm⁻¹ are in line with the intensity of these bands on the absolute spectra recorded before reaction (Figure 6 B, C versus Figure 1 A, C). The contribution at 1500–1670 cm⁻¹ (Figure 6 B) may be attributed to the presence of various types of carbon adsorbates. By comparing the samples with various stoichiometries activated at 623 K, it is found that the higher the perturbation of the bands related to OH emerging from the channels is, the higher the EtOH conversion is. This behavior is also valid when considering the perturbation of the POH areas. However, the intensity of the perturbation of the whole POH area recorded during reaction 1 does not match the absolute intensities of the POH area recorded after activation step (see HAp-O₆₂₃ K versus HAp-S₆₂₃ K in Figure 1C). Such a different behavior can be attributed to the fact that, as mentioned in the former section, the contribution at 3678 cm⁻¹, particularly intense for HAp-S₆₂₃ K is comparatively more perturbed than the POH contributions at lower wavenumbers. In the case of the HAp-O₈₇₃ K sample (SI 2, Figure S2), beside the absence of a negative signal at 1577 cm⁻¹ that confirms the release of unidentate carbonates at high temperature (red spectrum in Figure 6 B), the fraction of perturbed OH vibrators is not only much greater than that for HAp-O₆₂₃ K (comparison of green and red spectra in Figure 6 C), but also the most intense among all of the investigated samples. This confirms the correlation between the intensity of the perturbation of the OH contributions and the EtOH conversion. In addition, for HAp-O₈₇₃ K a broadening of the negative signal is also observed

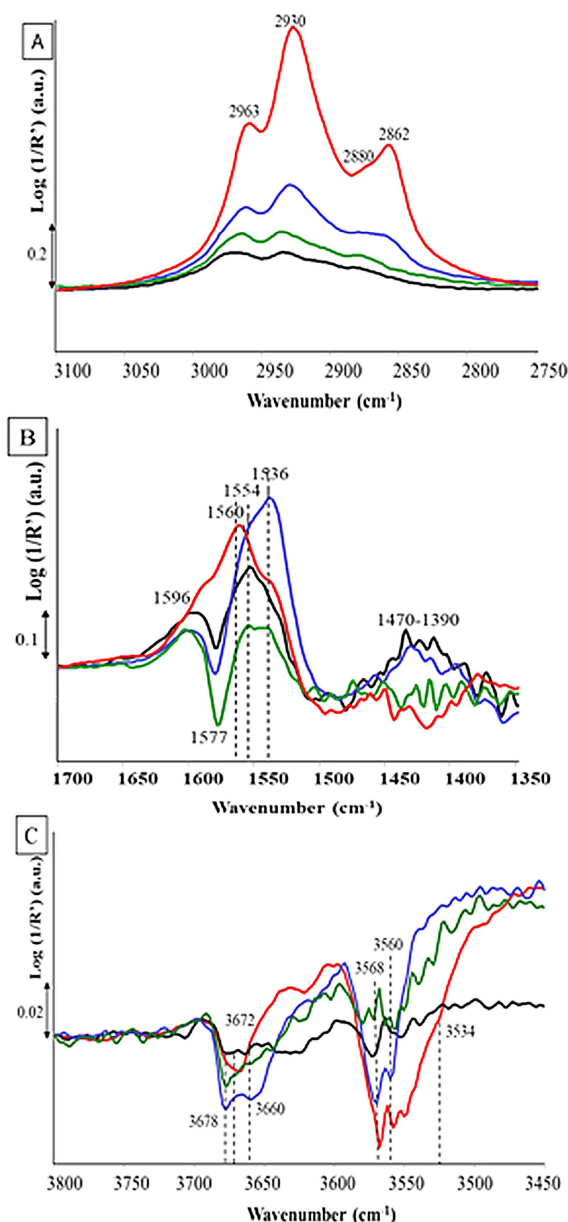


Figure 6. Difference DRIFT spectra recorded at the end of the reaction 1 step for the HAP-S_{623 K} (blue), HAP-U_{623 K} (black), HAP-O_{623 K} (green) and HAP-O_{873 K} samples (red) in the (A) ν_{CH} (B) ν_{CO} and (C) ν_{OH} regions.

with a perturbation of the contribution at 3534 cm^{-1} (indirectly related to the formation of O^{2-} species). This is in line with the relative increase of the 3534 cm^{-1} contribution compared to that at 3566 cm^{-1} observed upon increasing the temperature of the thermal pretreatment (see green and red spectra in Figure 1 B). This strongly suggests that, in addition to basic surface OH^- groups, the corresponding fraction of surface O^{2-} species (expected to be more basic) are also involved in the catalytic process. This might also account for the higher reactivity of the sample activated at the higher temperature for the MBOH reaction (SI 1 Figure S1a).

3. Evolution under He Flow

In order to evaluate the reversibility of the surface processes occurring during the reaction, ethanol was suddenly removed from the flow at 623 K .

3.1 Desorption of the Products Detected in Gas Phase

As shown in the case of the HAP-S_{623 K} sample in Figure 7, the amounts of acetaldehyde, *n*-butanol and ethanol detected in the gas phase progressively decrease. *n*-butanol is no longer observed after 35 min under He flow, whereas ethanol and acetaldehyde are still observed after 55 min on stream. Note also that few unidentified peaks, probably related to the desorption of some unidentified heavy products, were also detected.

3.2 State of the HAP Surfaces Monitored by DRIFT

3.2.1 Evolution of the Adsorbates

For all of the HAP samples, the intensity of the contributions associated to ν_{C-H} ($2800\text{--}3000\text{ cm}^{-1}$) decreases under helium flow.

After 2 hours under He flow, only about half of the C–H adsorbates formed during reaction 1 were released (Figure 8 A). In contrast, the intensity of the multi-components band at $1500\text{--}1650\text{ cm}^{-1}$ increases slightly under helium flow (Figure 8 B). This indicates that the corresponding carboxylates, which formation started during reaction 1 step, are strongly adsorbed. Moreover, even in the case of the HAP-O_{873 K} sample (SI 2 Figure S2) that is the only sample not exhibiting the characteristic band ascribed to unidentate calcium carbonates, a significant increase in the intensity of the $1596\text{--}1587\text{ cm}^{-1}$ signal assigned to ν_{CC} vibrators is observed (Figure 9 B), which indicates an increasing formation of carbon polymeric species under helium flow.

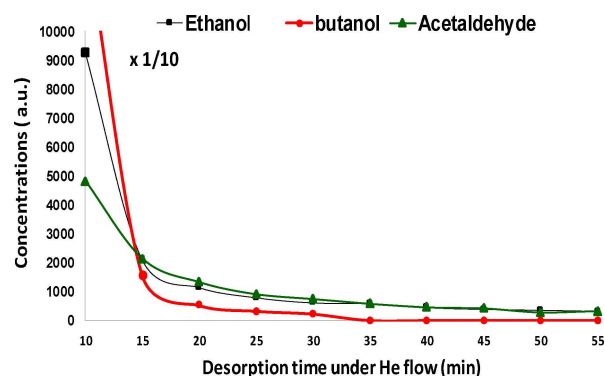


Figure 7. Evolution of the EtOH and the products concentrations in gas phase under helium flow for the HAP-S_{623 K} sample.

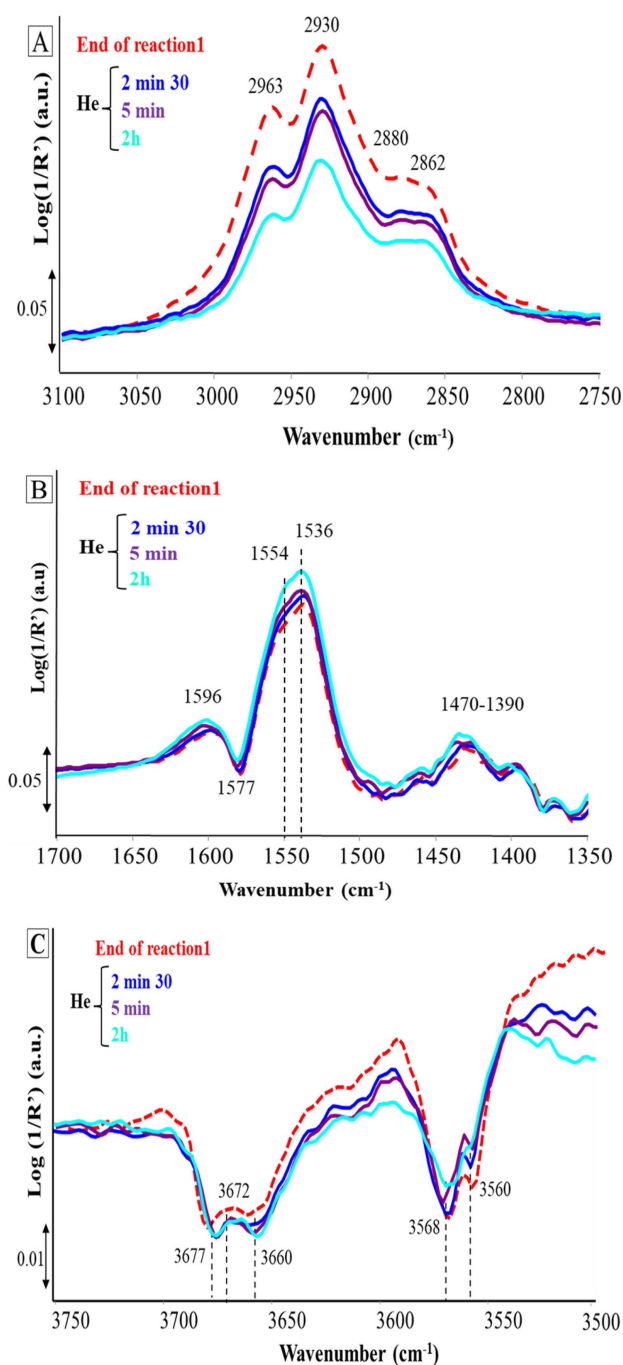


Figure 8. Difference DRIFT spectra recorded upon increasing exposure to He flow for the HAp-S_{623 K} sample in the (A) ν_{CH} (B) ν_{CO} and (C) ν_{OH} regions.

3.2.2 Poisoning and Regeneration of the Surface Sites?

For all of the samples, neither the unidentate calcium carbonates (when initially present) (Figures 8 B, 9 B) nor the surface POH groups (Figures 8 C, 9 C) are regenerated under He flow. Compared to the spectrum recorded at the end of the reaction 1 step, the POH vibrators are even slightly more perturbed over time under He flow (Figure 8 C). Such a perturbation of the POH groups under He flow is indicative of

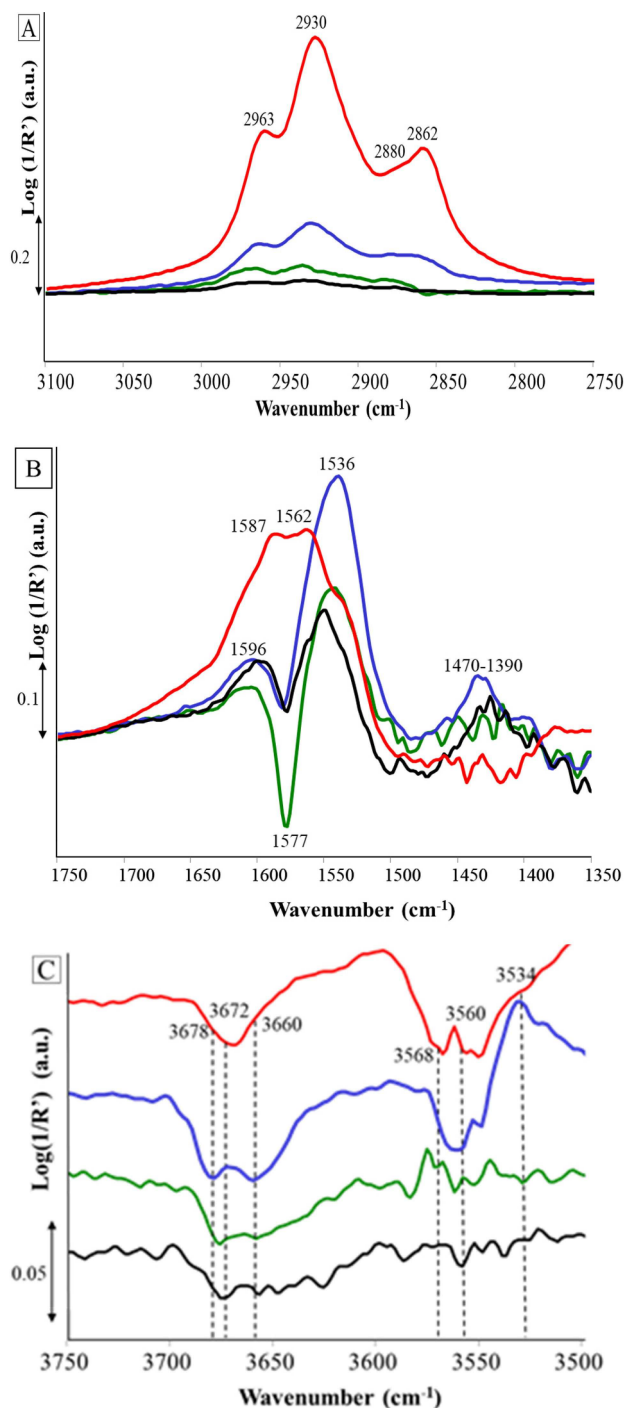


Figure 9. Difference DRIFT spectra recorded after 2 hours under He flow for HAp-S_{623 K} (blue), HAp-U_{623 K} (black), HAp-O_{623 K} (green) and HAp-O_{873 K} (red) in the (A) ν_{CH} (B) ν_{CO} and (C) ν_{OH} regions.

their strong interaction with the adsorbates formed under the reaction 1 step. This also shows that all of the POH groups have not been fully poisoned during the reaction 1 step and therefore remained available for the reaction.

Regarding the OH region, the perturbation of the OH bands occurred during reaction 1 decreases upon time under He flow (Figure 8 C and Figure 9 C), but at different extents depending

on the samples. In particular, the HAp-U_{623 K} and HAp-O_{623 K} samples do not show any negative contributions around 3570–3560 cm⁻¹ (flat baseline on the black and green difference spectra in Figure 9 C). This suggests that the OH⁻ groups previously present on the freshly activated samples have been fully regenerated under helium flow. Hence, contrary to surface POH groups and possibly surface unidentate calcium carbonates, the surface OH⁻ groups must not directly be involved in the formation of the carbon polymeric species.

Moreover, the possible full regeneration of the OH⁻ groups (Figure 9 C for HAp-U_{623 K} and HAp-O_{623 K}) in the absence of ethanol in the feed may indicate their involvement in the interaction with ethanol. In contrast, only a limited fraction of the perturbed surface OH⁻ groups at 3568 and 3560 cm⁻¹ has been recovered under helium flow for HAp-S_{623 K} and HAp-O_{873 K} samples (blue and red spectra in Figure 6 C and Figure 9 C). This is also the case for the 3534 cm⁻¹ contribution that is indirectly characteristic of the involvement of the O²⁻ species for HAp-O_{873 K}. OH⁻ (and O²⁻) sites were only partially regenerated under He flow in the case of the most reactive samples toward MBOH (HAp-O_{873 K} and HAp-S_{623 K}), but fully regenerated for the less active ones (HAp-O_{623 K} and HAp-U_{623 K}). The regeneration ability of surface OH⁻ sites of these hydroxapatite samples must therefore be correlated to the strength and/or density of the basic surface OH⁻ groups evaluated by the conversion of MBOH into acetone and acetylene (SI 1).

4. Reaction 2 Step

The initial surface state associated with the reaction 2 step (end of He flow step) is different from that associated with reaction 1 step (end of activation step). As seen above, modifications on the related surfaces occurred between these two steps (Figure 2). Unidentate calcium carbonates and POH groups are still present on the surface at the end of He flow step but no more accessible since they are now interacting strongly with adsorbed carbon polymeric species (Figure 2 B). Compared with the end of the activation step, basic OH⁻ sites are present either in similar amounts (for HAp-U_{623 K} and HAp-O_{623 K}) or in lower amounts (for HAp-S_{623 K} and HAp-O_{873 K}). Let us examine how such modifications influence the surface reactivity.

4.1 Gas Phase Analysis

4.1.1 Ability to Recover the EtOH Conversion

As reported in Figure 10, the ability of the samples to recover an initial conversion of ethanol during reaction 2 step comparable to that measured during the reaction 1 step is different from one sample to another. Ethanol conversion is fully recovered for HAp-U_{623 K} and HAp-O_{623 K}, whereas a significant loss of conversion is observed for HAp-S_{623 K} and HAp-O_{873 K}. Given that both POH groups and unidentate carbonates (when present for samples activated at 623 K) are poisoned for all of the samples, none of these surface sites

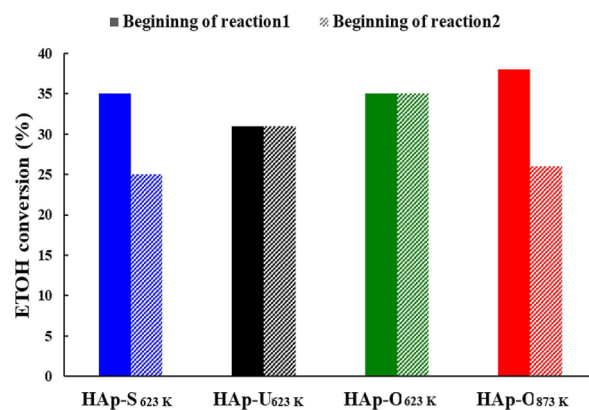


Figure 10. Comparison of the initial ethanol conversions between reaction 1 and reaction 2 steps for the HAp samples.

must be directly involved in the activation of ethanol. Interestingly, the fraction of ethanol conversion recovered during the reaction 2 step appears to be directly related to the fraction of surface OH⁻ groups recovered upon the He step. Indeed, HAp-U_{623 K} and HAp-O_{623 K} show a full regeneration of the surface OH⁻ groups upon the He step (Figure 9 C) together with a full recovery of the initial ethanol conversion in reaction 2 step. In contrast, HAp-S_{623 K} and HAp-O_{873 K} show a partial regeneration of the OH⁻ (and derived O²⁻) groups after the He step (Figure 9 C) and a decrease in the initial ethanol conversion in reaction 2 step (25% initial ethanol conversion in the reaction step 2 versus 35% in the reaction step 1 over HAp-S_{623 K}, Figure 10). Hence, this shows that the conversion of ethanol on the HAp surface is clearly governed by the density and/or the strength of the surface basic OH⁻ (and derived O²⁻-species) groups. Such an involvement of the OH⁻ sites as active sites of the conversion of ethanol over HAp is also supported by the much lower activity and *n*-butanol selectivity obtained for other calcium phosphate phases that do not exhibit basic OH⁻ groups, such as beta tricalcium phosphate, fluorapatite^[23] and octacalcium phosphate^[30] that also exhibit poor basicity compared to HAp.^[23,30]

4.1.2 Impact on the Selectivity

Regardless of whether the ethanol conversion has been fully recovered or not, the products selectivities in reaction 2 step were found to be greatly modified compared to reaction 1 step. For all of the samples, as illustrated for HAp-S_{623 K} and HAp-U_{623 K} in Figure 11 A and B, the production of *n*-butanol and acetaldehyde in the reaction 2 step are greatly modified.

From the beginning of reaction 2 step, *n*-butanol is hardly produced, while the production of acetaldehyde is drastically increased compared to reaction 1 step. Such a sharp increase in acetaldehyde production during reaction 2 step is the most pronounced for HAp-U_{623 K} by about a two-fold increase compared to other samples (Figure 11 B). In parallel, hydrogen concentration remained quite limited during reaction 1 step, as

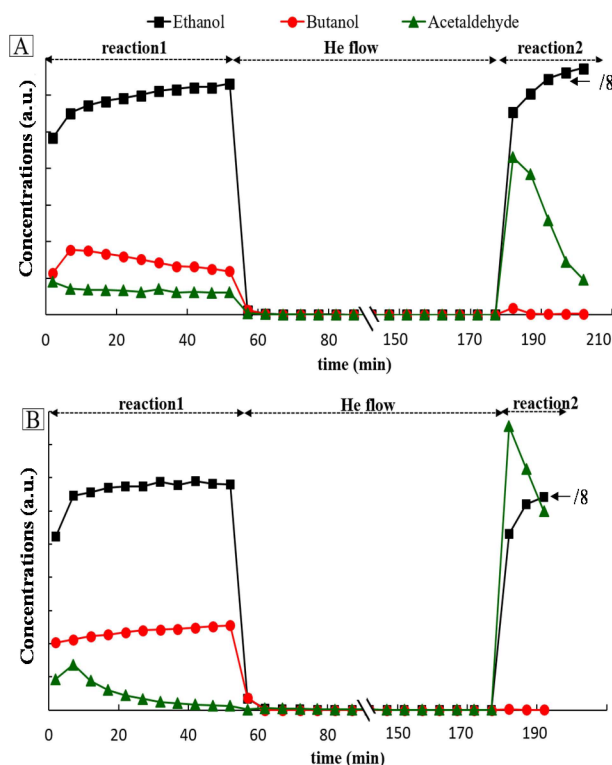


Figure 11. Evolution of the concentrations in ethanol, *n*-butanol and acetaldehyde evolved during the successive steps for A) HAP-S_{623 K} and B) HAP-U_{623 K} samples.

expected from its production upon the dehydrogenation step of ethanol to acetaldehyde, whereas a sharp increase in its concentration was observed during reaction 2 step (not shown).

4.2. Nature of the Acidic Sites Involved in the Key Reactions Steps

Such changes in the selectivity profiles between reaction steps 1 and 2 indicate that different active sites must be involved in the relevant key reaction steps, i.e. dehydrogenation for acetaldehyde formation and subsequent aldol condensation for *n*-butanol formation. Such a conclusion is in accordance with that already drawn by Ho et al.^[4b]

On HAP-S_{623 K}, the intensity of ν_{CH} contributions (Figure 12 A) increases during the reaction 2 step and remains of lower intensity compared to those achieved at the end of the reaction 1 step. This lower concentration of adsorbed products is consistent with the lower ethanol conversion recorded during reaction 2 step compared to reaction 1 step (Figures 10 and 11 A). In contrast, contributions associated to the presence of carbon polymeric species (1500–1650 cm^{-1}) (Figure 12 B) increase continuously. The perturbed bands related to POH sites are not modified upon the introduction of ethanol during the reaction 2 step (Figure 12 C). This confirms that the POH groups have already been fully poisoned during the He step, as mentioned in the previous section. Hence, in the absence of

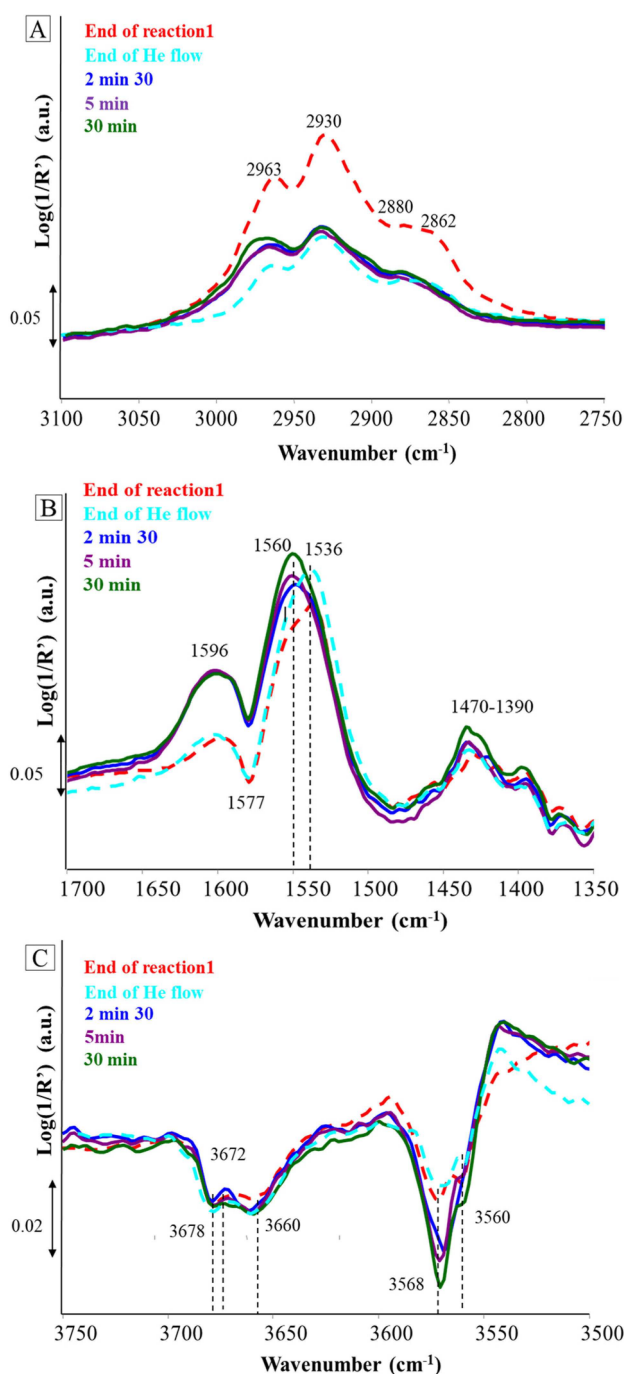


Figure 12. Difference DRIFT spectra recorded for HAP-S_{623 K} sample from the beginning of reaction 2 step in the (A) ν_{CH} (B) ν_{CO} and (C) ν_{OH} regions.

regeneration of the surface POH acid sites (not recovered under He flow), it is likely that the few Ca^{2+} cations accessible on the surface still contribute to the reaction together with the regenerated surface basic OH^- groups, as illustrated by the perturbation observed at $\sim 3568 \text{ cm}^{-1}$ in Figure 12 C, finally promoting the formation of acetaldehyde. Whereas two negative contributions of similar intensity were observed at 3568 and 3560 cm^{-1} at the end of reaction 1 step (Figure 4 C), Figure 12 C shows that the band at 3568 cm^{-1} is much more

intense than that at 3560 cm^{-1} in reaction 2 step. Even if DFT calculations would be required to assess the origin of these two surface OH^- contributions, this result may be an indication that the 3568 cm^{-1} contribution is characteristic of surface basic OH^- groups acting cooperatively with Ca^{2+} ions as an acidic partner (whereas that at 3560 cm^{-1} may correspond to OH^- groups acting together with POH groups).

Such a trend is also observed for the other samples (Figure 13) (SI 2), except for HAP- $\text{U}_{623\text{ K}}$ (see black spectra in Figure 13 B and C). For this latter sample, as the reaction 2 step starts, most carbon polymeric species (bands in the $1500\text{--}1670\text{ cm}^{-1}$ region) suddenly vanished unexpectedly, may be due to an uncontrolled exothermic process. Simultaneously, the underlying surface POH groups were also suddenly recovered (flat baseline in the corresponding area of the black spectrum in Figure 13 C) and the unidentate calcium carbonate contribution (band at 1577 cm^{-1}) disappeared, as shown on the absolute DRIFT spectrum reported in Figure 14 and the absence of the corresponding negative contribution in Figure 14 B. More importantly, despite the full regeneration of the POH and OH^- groups for HAP- $\text{U}_{623\text{ K}}$, the product selectivities related to reaction 2 step once more differ from those obtained during reaction 1 step, with a significant increase in the acetaldehyde production (Figure 11 B). The IR contribution related to surface basic OH^- sites is once again perturbed, with a single negative contribution at 3568 cm^{-1} (Figure 13 C) and the surface POH species remain as spectators species during the reaction 2 step, as illustrated by the flat baseline observed in the related regions in Figure 13 C. Such an increase in acetaldehyde production in reaction 2 step over HAP- $\text{U}_{623\text{ K}}$ (Figure 11 B) can be explained by the prevailing involvement of Ca^{2+} cations whose accessible amount was strongly increased due to the release of the corresponding unidentate carbonates. Hence, Ca^{2+} cations acting together with OH^- groups (either because POH groups have been previously poisoned or because their relative amount is increased) favor the formation of acetaldehyde. Such ability of the $\text{Ca}^{2+}\text{--OH}^-$ pair to favor the formation of acetaldehyde is supported by the previous work of Tsuchida et al.^[3a] in which it was shown that the prevailing formation of acetaldehyde from ethanol was favored on CaO (that also exposes $\text{Ca}^{2+}\text{--OH}^-$ pairs under the related operating conditions^[31]). In contrast, *n*-butanol can be formed as long as a fraction of POH groups keeps on working (reaction 1 step).

How can it be considered that different acidic partners, Ca^{2+} and POH species would be involved in the dehydrogenation and aldol condensation key reaction steps? Firstly, the strength of the acidic site partner of the deprotonating basic site plays a key role in basic reactions for the stabilization of the anionic intermediate (here, Ca^{2+} is a stronger acidic site than POH sites). More specifically in the case of the aldol condensation, it was underlined that a peculiar acid-base balance is required.^[32] Secondly, besides the relative strength, the respective Lewis and Brønsted nature of the two acidic sites needs to be taken into consideration. On the one hand, in the case of dehydrogenation of primary or secondary alcohol (such as isopropanol), both a deprotonating basic site and a Lewis acid site are required to form the alcoholate intermediate and to abstract

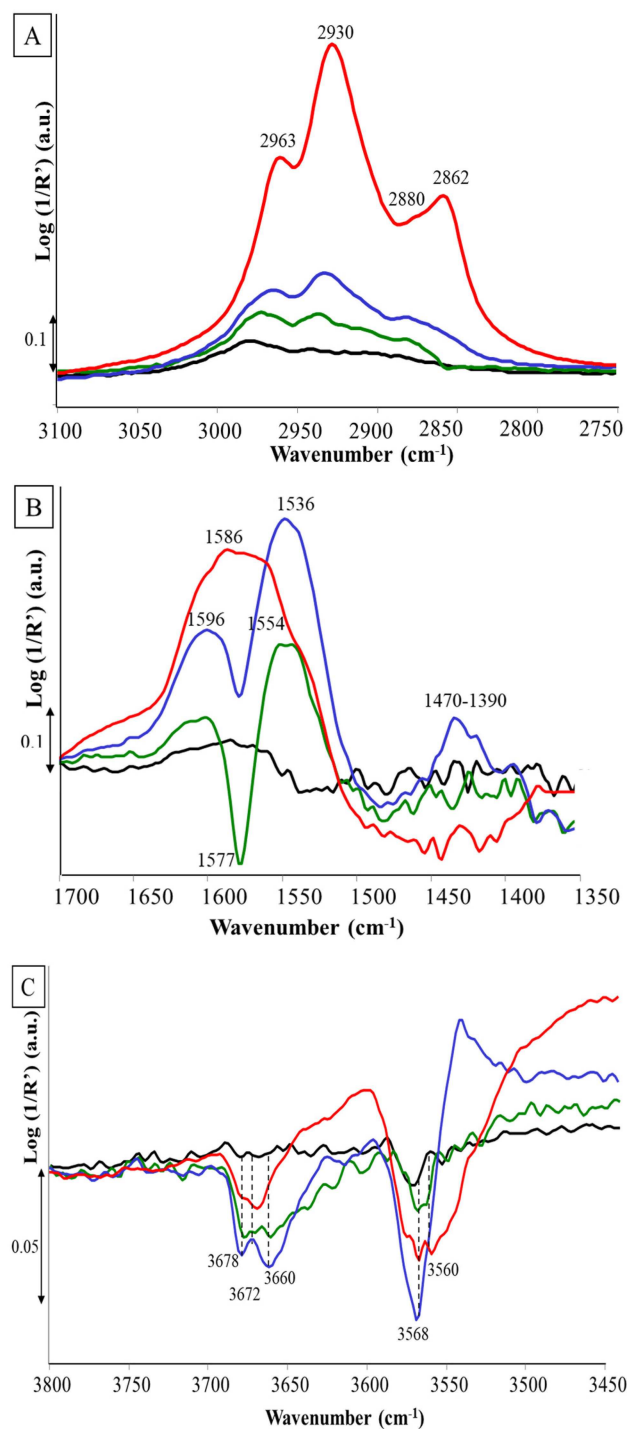


Figure 13. Difference DRIFT spectra recorded for HAP- $\text{S}_{623\text{ K}}$ (blue), HAP- $\text{O}_{623\text{ K}}$ (green), HAP- $\text{O}_{873\text{ K}}$ (red) and HAP- $\text{U}_{623\text{ K}}$ (black) samples from the beginning of reaction 2 step in the (A) ν_{CH} (B) ν_{CO} and (C) ν_{OH} regions.

the hydride ion, respectively.^[22b] On the other hand, Brønsted acid sites were proposed to be involved in the formation of crotonaldehyde from acetaldehyde.^[33]

Compared to other basic catalytic systems, hydroxyapatite is the only catalyst to exhibit both Lewis (Ca^{2+}) and Brønsted (POH) acid sites likely to act as acidic partners of the acid-base

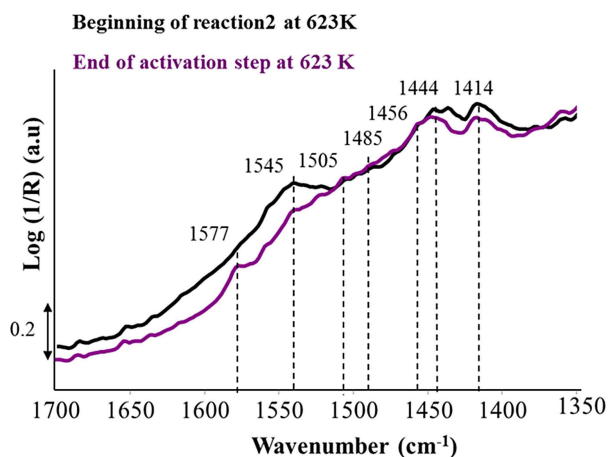


Figure 14. Absolute spectra recorded for HAp-U_{623 K} sample at the end of the activation step and at the beginning of the reaction 2 step in the ν_{CO} region.

pairs involved in the two first steps of *n*-butanol formation, namely the dehydrogenation of ethanol and the aldol condensation steps. In combination with the basic sites, mainly OH⁻ groups under the present operating conditions, but also the few derived O²⁻ species present when high thermal treatment is performed, these acidic sites provide two acid-base pairs able to form acetaldehyde and to further transform it via hydride aldol condensation. Finally, another key reaction step to produce *n*-butanol from ethanol is the hydrogenation of crotonaldehyde into *n*-butanol.^[7a] It remains unclear at present whether the recombination of the species (stored on Ca²⁺ ions) with protons (particularly available for this proton conductor material^[25b]) may explain the peculiar ability of hydroxyapatite to achieve by itself this last hydrogenation step, whereas other traditional basic systems always require the addition of a metallic function to selectively produce *n*-butanol. If the involvement of MPV-like mechanism is proposed,^[10] the role of the proton mobility on the catalytic behavior of hydroxyapatite will also be discussed in a forthcoming paper.

Conclusions

Operando DRIFT study was carried out to follow the catalytic transformation of ethanol into acetaldehyde and *n*-butanol, and to identify the nature and the role of the active sites. Apart from the formation of positive IR contributions in difference spectra attributed to the presence of strongly-bound carbon polymeric species, responsible for the observed deactivation process, peculiar attention was devoted to the changes in the negative contributions related to the perturbation of surface vibrators. The ability of such sites to be recovered under an He atmosphere and their consequence on a second reaction step were investigated. Among the surface sites, unidentate calcium carbonates, terminated POH and OH groups emerging from the columns, only the basic OH groups could be partially or fully (for the most basic ones) regenerated under the He step, resulting in the partial or full recovery of the initial ethanol

conversion during a subsequent second reaction step. This clearly shows that the availability of the basic OH⁻ groups governs the activation of ethanol. The promoting effect of the high activation temperature (873 K) of HAp on the ethanol conversion measured at 623 K is ascribed to the presence of few strong O²⁻ basic sites derived from the dehydroxylation of columnar OH⁻ groups that are involved in the activation of ethanol. The existence of two surface OH contributions may refer to the involvement of two types of surface OH⁻ groups, with up and down orientations of their protons, that would react differently with their neighboring acidic partners, namely Ca²⁺ and POH species. The nature of the acidic sites acting cooperatively with these OH⁻ groups within acid-base pairs required for any basic reaction steps is determinant to control the selectivity in the formed products: 1) *n*-butanol is formed only as long as POH sites are still available, 2) once the POH sites have been poisoned (upon intermediate treatment under He) and a higher number of Ca²⁺ species is accessible (resulting from the release of unidentate carbonates), only Ca²⁺ cations are involved as an acidic partner of the basic OH⁻ groups. Hence, the acid-base pair involved in the transformation of ethanol switches to Ca²⁺-OH⁻ during reaction 2 step, and the reaction leads mainly to the formation of acetaldehyde. This not only confirms that acetaldehyde acts as an intermediate in the formation of *n*-butanol, but also indicates that various active sites are involved in the relevant key reaction steps: Ca²⁺-OH⁻ and POH-OH⁻ as acid-base pairs in the dehydrogenation of ethanol to acetaldehyde and the aldol condensation for *n*-butanol formation, respectively. The simultaneous availability of two weak acid-base pairs on a single material, also including Lewis acid sites favoring hydride abstraction to dehydrogenate ethanol and Brønsted acid sites favoring the aldol condensation reaction, makes hydroxyapatite a unique catalytic system able to transform selectively ethanol to *n*-butanol without the need of any metallic function.

Experimental Section

Sample Preparation and Characterization

Hydroxyapatite samples were prepared according to the procedure described previously:^[30] the co-precipitation of Ca(NO₃)₂ and (NH₄)₂HPO₄ solutions beforehand adjusted at pH=10 was performed at 353 K under a N₂ flow to limit carbonation of the materials. As detailed elsewhere,^[14b] depending on the pH control procedures, even with a nominal Ca/P ratio of 1.67 of the precursors in the solutions, hydroxyapatite samples can be obtained with different Ca/P ratios. The three HAp samples studied in this work have been obtained by periodic, continuous or without addition of NH₄OH during the precipitation step, respectively. The obtained precipitates were then matured at the same temperature for 4 hours under reflux. The washed precipitates were then dried overnight at 373 K and thermally treated under Ar flow (150 mL min⁻¹) up to 623 K (5 K min⁻¹) for 90 min. In one case, a thermal treatment was also carried out at 873 K. The Ca/P ratios measured by ICP-AES analysis ("Service Central d'Analyse" of the CNRS, Solaize, France) were 1.67, 1.77 and 1.64, for the samples prepared with periodic, continuous or without addition of NH₄OH, respectively. The samples will be hereafter referred to as HAp-S_{623 K}.

HAP-O_{623 K}, HAP-O_{873 K} and HAP-U_{623 K}, respectively, where S, O and U stand for stoichiometric, over-stoichiometric and under-stoichiometric Ca/P ratios, respectively, and 623 and 873 K refer to as the temperatures of final thermal treatment applied for the various samples (the same temperature is further applied for activation step performed prior to catalytic measurements).

X-ray powder diffractograms were recorded with a D8 Advance diffractometer equipped with a Copper anode generator ($\lambda = 1.5418 \text{ \AA}$). Diffractograms were recorded by 0.02° steps in the 2θ range of $10\text{--}85^\circ$. The crystalline hydroxyapatite structure of the samples was identified from comparison with the ICDD pattern 01-074-9780(A). Specific surface areas were measured by adsorption of N_2 at 77 K on a Micromeritics (ASAP 2010) apparatus and calculated from the BET method. After thermal treatment at 623 K, HAP-S_{623 K}, HAP-O_{623 K} and HAP-U_{623 K} exhibit specific surface areas of 41, 42 and $31 \text{ m}^2 \text{ g}^{-1}$, respectively. Thermal treatment of sample HAP-O at 873 K (HAP-O_{873 K}) leads to a decrease in the specific surface area down to $33 \text{ m}^2 \text{ g}^{-1}$. The *in situ* characterization of the acidity of these materials was detailed elsewhere^[7e] from the adsorption of CO at 77 K monitored by infra-red. It was shown that the accessibility of Ca^{2+} ions exposed at the top surface of HAP-S_{623 K}, HAP-U_{623 K}, HAP-O_{623 K} and HAP-O_{873 K} remained quite limited compared to that of terminal POH groups.

Operando DRIFT Experiments

The HAP samples (40 mg) were placed inside a heated crucible located in a Thermo Spectra-Tech high-temperature cell equipped with ZnSe windows and with appropriate gas inlet and outlet connections as to pass the gas flow through the catalytic bed and to ensure homogenous contact between the sample and the flowing gas.^[32a,34] Successive steps were considered, as summarized in Figure 15. After activation, a first reaction step (reaction 1) was carried out for one hour at 623 K. The reactant feed was then switched to He flow for 2 hours, maintaining the temperature at 623 K. Finally, a second reaction step (reaction 2) was carried out at the same temperature.

The activation of the samples was carried out under helium flow (20 mL min^{-1}), heating the sample (5 K min^{-1}) up to 623 or 873 K, and maintaining this temperature for 90 min, before switching from the inert flow to the reactant feed. The reactant feed consisted of ethanol diluted in He. Helium (20 mL min^{-1}) was bubbled in ethanol (Aldrich, 99.9%) at 278 K to achieve a contact time of $37 \text{ g}_{\text{cat.}}/\text{h/mol ethanol}$. A flow of 20 mL min^{-1} was maintained during the intermediate step under He.

The gas phase composition at the exit of the DRIFT cell was analyzed every 5 min using a two channels micro-gas chromatograph (Varian, CP4900) equipped with PPQ and 5CB columns allowing the separation and the catharometric quantification of

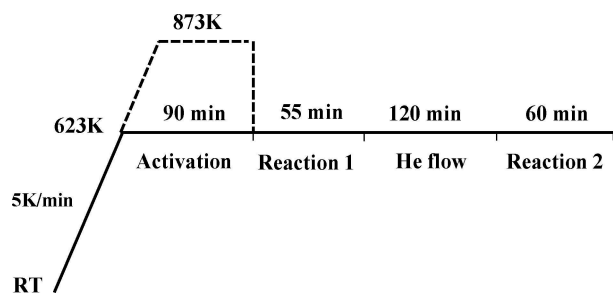


Figure 15. Sequence of successive steps implemented under *operando* conditions (the dashed line refers to as the pretreatment achieved in the case of HAP-O_{873 K}).

light and heavy products, respectively. EtOH conversion and selectivities were calculated as follows: $\text{conv}_{\text{EtOH}} (\%) = (\text{P}_{\text{EtOH}}^\circ - \text{P}_{\text{EtOH}}) \times 100 / \text{P}_{\text{EtOH}}^\circ$, $\text{Sel}_i (\%) = \alpha_i \text{P}_i \times 100 / (\text{P}_{\text{EtOH}}^\circ - \text{P}_{\text{EtOH}})$, where $\text{P}_{\text{EtOH}}^\circ$ is the reference EtOH pressure measured before reaction, P_{EtOH} and P_i are partial pressures of EtOH and *i* product during the reaction and α_i the $1/2$ of the number of carbon in the *i* product.

Diffuse reflectance infrared spectra were recorded in the $4000\text{--}1200 \text{ cm}^{-1}$ range (4 cm^{-1} resolution, 256 scans/spectrum, MCT detector) using a Brüker IFS 66 V spectrometer every 150 s. A reference spectrum was recorded with KBr (Fluka, purity $>99.5\%$) under the same operating conditions. The absolute spectra recorded at the end of the activation step (623 or 873 K) are reported in $\log 1/R$ with $R = I_{\text{HAP}}/I_{\text{KBr}}$. The difference DRIFT spectra reported for the successive steps of the sequence are reported in $\log 1/R'$ with the relative reflectance $R' = I_{\text{HAP sequence}}/I_{\text{HAP}}$ (spectrum recorded during the successive steps of the sequence/spectrum recorded at 623 or 873 K at the end of the activation step).^[35] The gas phase contribution of ethanol was systematically subtracted for spectra related to the two reaction steps. No significant modification of the shape nor intensity of the P–O combination bands ($2200\text{--}1950 \text{ cm}^{-1}$) were observed during the successive investigated steps performed at 623 K, which indicates that the optical properties of the samples are not modified during the reaction processes. For comparison purpose, when spectra related to different samples are reported on a same Figure, normalization using the P–O combination bands has been systematically applied.

Acknowledgements

The authors are grateful to Vincent Lhosinho from the Laboratoire de Réactivité de Surface, Sorbonne Université, for his help in the maintenance of the EtOH and MBOH reaction set-up.

Conflict of Interest

The authors declare no conflict of interest.

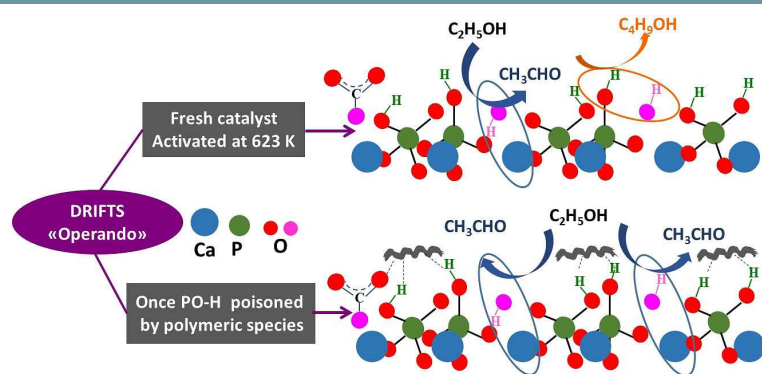
Keywords: POH/OH[−] and Ca²⁺/OH[−] acid base pairs • DRIFT • hydroxyapatites • operando

- [1] a) G. R. M. Dowson, M. F. Haddow, J. Lee, R. L. Wingad, D. F. Wass, *Angew. Chem. Int. Ed.* **2013**, *52*, 9005–9008; *Angew. Chem.* **2013**, *125*, 9175–9178; b) J. Sun, Y. Wang, *ACS Catal.* **2014**, *4*, 1078–1090.
- [2] D. L. Carvalho, R. R. d. Aveliz, M. T. Rodrigues, L. E. P. Borges, L. G. Appel, *Appl. Catal. A* **2012**, *415–416*, 96–100.
- [3] a) T. Tsuchida, T. Yoshioka, S. Sakuma, T. Takeguchi, W. Ueda, *Ind. Eng. Chem. Res.* **2008**, *47*, 1443–1452; b) N. Savage, *Nature* **2011**, *474*, S9–S11.
- [4] a) S. Hanspal, Z. D. Young, H. Shou, R. J. Davis, *ACS Catal.* **2015**, *5*, 1737–1746; b) C. R. Ho, S. Shylesh, A. T. Bell, *ACS Catal.* **2016**, *6*, 939–948.
- [5] K. Koda, T. Matsu-ura, Y. Obara, Y. Ishii, *Chem. Lett.* **2009**, *38*, 838–839.
- [6] a) T. Tsuchida, S. Sakuma, T. Takeguchi, W. Ueda, *Ind. Eng. Chem. Res.* **2006**, *45*, 8634–8642; b) J. T. Kozlowski, R. J. Davis, *ACS Catal.* **2013**, *3*, 1588–1600; c) D. Gabriëls, W. Y. Hernández, B. Sels, P. Van Der Voort, A. Verberckmoes, *Catal. Sci. Technol.* **2015**, *5*, 3876–3902.
- [7] a) T. Tsuchida, J. Kubo, T. Yoshioka, S. Sakuma, T. Takeguchi, W. Ueda, *J. Catal.* **2008**, *259*, 183–189; b) S. Ogo, A. Onda, Y. K., *Appl. Catal. A* **2011**, *402*, 188–195; c) J. Scalbert, F. Thibault-Starzyk, R. Jacquot, D. Morvan, F. Meunier, *J. Catal.* **2014**, *311*, 28–32; d) L. Silvester, J. F. Lamonier, Faye, J., M. Capron, R. N. Vannier, C. Lamonier, J. L. Dubois, J. L. Couturier, C. Calais, F. Dumeignil, *Catal. Sci. Technol.* **2015**, *5*, 2994–3006; e) M. Ben Osman, S. Diallo Garcia, J. M. Krafft, C. Methivier, J. Blanchard, T.

- Yoshioka, J. Kubo, G. Costentin, *Phys. Chem. Chem. Phys.* **2016**, *18*, 2783–27847.
- [8] M. Guerbet, *C. R. Chim.* **1909**, *149*, 129.
- [9] a) S. Veibel, J. I. Nielsen, *Tetrahedron* **1967**, *213*, 1723–1733; b) A. J. O'Lenick, *J. Surfactants Deterg.* **2001**, *4*, 311–315; c) C. Carlini, M. Di Girolamo, A. Macinai, M. Marchionna, M. Novello, A. M. Raspolti Galletti, G. Sbrana, *J. Mol. Catal.* **2003**, *200*, 137–146.
- [10] Z. D. Young, R. J. Davis, *Catal. Sci. Technol.* **2018**, *8*, 1722–1729.
- [11] M. J. L. Gines, E. Iglesia, *J. Catal.* **1998**, *176*, 155–172.
- [12] a) S. Sugiyama, Y. Iguchi, T. Minami, H. Hayashi, J. B. Moffat, *Catal. Lett.* **1997**, *46*, 279–285; b) S. Sugiyama, E. Nitta, H. Hayashi, J. B. Moffat, *Catal. Lett.* **1999**, *59*, 67–72; c) S. Sugiyama, T. Osaka, Y. Hirata, K. I. Sotowa, *Appl. Catal. A* **2006**, *312*, 52–58.
- [13] a) S. J. Joris, C. H. Amberg, *J. Phys. Chem.* **1971**, *75*, 3167–3171; b) H. Monma, *J. Catal.* **1982**, *75*, 200–203; c) M. Zahouily, Y. Abrouki, B. Bahlaouan, A. Rayadh, S. Sebti, *Catal. Commun.* **2003**, *4*, 521–524; d) S. Sebti, A. Solhy, R. Tahir, A. Smahi, *Appl. Catal. A* **2002**, *235*, 273–281; e) A. Solhy, J. H. Clark, R. Tahir, S. Sebti, M. Larzek, *Green Chem.* **2006**, *8*, 871–874.
- [14] a) T. Tsuchida, J. Kubo, T. Yoshioka, S. Sakuma, T. Takeguchi, W. Ueda, *J. Jap. Petrol. Inst.* **2009**, *52*; b) M. Ben Osman, J. M. Krafft, Y. Millot, F. Averseng, T. Yoshioka, J. Kubo, G. Costentin, *Eur. J. Inorg. Chem.* **2016**, *2016*, 2709–2720.
- [15] a) S. Ogo, A. Onda, K. Yanagisawa, *Appl. Catal. A* **2008**, *348*, 129–134; b) L. Silvester, J. F. Lamontier, R. N. Vannier, C. Lamontier, M. Capron, A. S. Mamede, F. Pourpoint, A. Gervasini, F. Dumeignil, *J. Mater. Chem. A* **2014**, *2*, 11073–11090; c) B. Yan, L. Z. Tao, Y. Liang, B. Q. Xu, *ACS Catal.* **2014**, *4*, 1931–1943; d) V. C. Ghantani, S. T. Lomate, M. K. Dongare, S. B. Umbarkar, *Green Chem.* **2013**, *15*, 1211–1217.
- [16] a) C. L. Kibby, K. W. Hall, *J. Catal.* **1973**, *31*, 65–73; b) A. Yasukawa, S. Ouchi, K. Kandori, T. Ishikawa, *J. Mater. Chem.* **1996**, *6*, 1401–1405; c) N. Cheikh, M. Kacimi, M. Rouimi, M. Ziyad, L. F. Liotta, G. Pantaleo, G. Deganello, *J. Catal.* **2005**, *232*, 257–267.
- [17] S. Diallo-Garcia, M. Ben Osman, J. M. Krafft, S. Casale, C. Thomas, J. Kubo, G. Costentin, *J. Phys. Chem. C* **2014**, *118*, 12744–12757.
- [18] a) S. Diallo-Garcia, M. Ben Osman, J. M. Krafft, S. Boujday, G. Costentin, *Catal. Today* **2014**, *226*, 81–88; b) M. Ben Osman, S. Diallo-Garcia, V. Herledan, T. Yoshioka, K. Kubo, Y. Millot, G. Costentin, *J. Phys. Chem. C* **2015**, *119*, 23008–23020.
- [19] C. Chizallet, M. L. Bailly, G. Costentin, H. Lauron-Pernot, J. M. Krafft, P. Bazin, J. Saussey, M. Che, *Catal. Today* **2006**, *116*, 196–205.
- [20] C. A. Ospina, J. Terra, A. J. Ramirez, M. Farinac, D. E. Ellis, A. M. Rossi, *Colloids Surf B: Biointerfaces* **2012**, *89*, 15–22.
- [21] a) R. M. Wilson, J. C. Elliot, S. E. P. Dowker, *J. Solid State Chem.* **2003**, *174*, 132–140; b) M. Jarlbring, D. E. Sandström, O. N. Antzutkin, W. Forsling, *Langmuir* **2006**, *22*, 4787–4792.
- [22] a) H. Lauron-Pernot, F. Luck, J. M. Popa, *Appl. Catal. A. Gen* **1991**, *78*, 213–225; b) H. Lauron-Pernot, *Catal. Rev.* **2006**, *48*, 315–361.
- [23] S. Hanspal, D. Young, J. T. Prillaman, R. J. Davis, *J. Catal.* **2017**, *352*, 182–190.
- [24] R. Philipp, K. Fujimoto, *J. Phys. Chem.* **1992**, *96*, 9035–9038.
- [25] a) C. Rey, J. C. Trombe, G. Montel, *J. Inorg. Nucl. Chem.* **1978**, *40*, 27–30; b) S. Nakamura, H. Takeda, K. Yamashita, *J. Appl. Phys.* **2001**, *89*, 5386; c) M. Yashima, Y. Yonehara, H. Fujimori, *J. Phys. Chem. C* **2011**, *115*, 25077–25087; d) N. Horiuchi, M. Nakamura, A. Nagai, K. Katayama, K. Yamashita, *J. Appl. Phys.* **2012**, *112*, 074901–074906.
- [26] a) N. W. Cant, J. A. S. Bett, G. R. Wilson, W. K. Hall, *Spectrochim. Acta* **1971**, *27A*, 425–439; b) F. Freund, R. M. Knobel, *J. C. S. Dalton* **1977**, 1136–1140.
- [27] a) S. Sugiyama, H. Hayashi, *Int. J. Mod. Phys. B* **2003**, *17*, 1476–1481; b) S. Sugiyama, T. Shono, D. Makino, T. Moriga, H. Hayashi, *J. Catal.* **2003**, *214*, 8–14.
- [28] a) T. W. Birky, J. T. Kozlowski, R. J. Davis, *J. Catal.* **2013**, *298*, 130–137; b) H. Idriss, *Platinum Met. Rev.* **2004**, *48*, 105–115; c) R. M. B. Faria, D. V. Cesar, V. M. M. Salim, *Catal. Today* **2008**, *133–135*, 168–173.
- [29] J. Datka, Z. Sarbak, R. P. Eischens, *J. Catal.* **1994**, *145*, 544–550.
- [30] S. Diallo-Garcia, D. Laurencin, J. M. Krafft, S. Casale, M. E. Smith, H. Lauron-Pernot, G. Costentin, *J. Phys. Chem. C* **2011**, *115*, 24317–24327.
- [31] H. Petitjean, J. M. Krafft, M. Che, H. Lauron Pernot, G. Costentin, *Phys Chem Phys* **2010**, *12*, 14740–14748.
- [32] a) J. F. Groust, G. Costentin, J. M. Krafft, P. Massiani, *Phys. Chem. Chem. Phys.* **2010**, *12*, 937–946; b) Y. C. Chang, A. N. Ko, *Appl. Catal. A* **2000**, *190*, 149–155; c) V. V. Ordonsky, V. L. Sushkevich, I. I. Ivanova, *J. Mol. Catal. A* **2010**, *333*, 85–93.
- [33] A. I. Biaglow, J. Sepa, R. J. Gorte, D. White, *J. Catal.* **1995**, *151*, 373–384.
- [34] C. Drouilly, J. M. Krafft, F. Averseng, H. Lauron-Pernot, D. Bazer-Bachi, C. Chizallet, V. Lecocq, *Catal. Today* **2013**, *205*, 67–75.
- [35] J. Sirita, S. Phanichphant, F. C. Meunier, *Anal. Chem.* **2007**, *79*, 3912–3918.

Manuscript received: November 16, 2018
Revised manuscript received: January 14, 2019
Accepted manuscript online: January 15, 2019
Version of record online: ■■■, ■■■■

FULL PAPERS



M. B. Osman, J.-M. Krafft, C. Thomas,
T. Yoshioka, J. Kubo, G. Costentin*

1 – 15

Importance of the Nature of the
Active Acid/Base Pairs of Hydrox-
yapatite Involved in the Catalytic
Transformation of Ethanol to *n*-
Butanol Revealed by *Operando*
DRIFTS



Drifting away. Atypical active sites were revealed on hydroxyapatite catalysts: $Ca^{2+}-OH^-$ and $POH-OH^-$ are proposed to act as acid-base pairs

in the dehydrogenation of ethanol to acetaldehyde and the aldol condensation for *n*-butanol formation, respectively.